NUMERICAL COUPLING OF ELECTRIC CIRCUIT EQUATIONS AND ENERGY-TRANSPORT MODELS FOR SEMICONDUCTORS*

MARKUS BRUNK† AND ANSGAR JÜNGEL†,‡

Abstract. A coupled semiconductor–circuit model including thermal effects is proposed. The charged particle flow in the semiconductor devices is described by the energy-transport equations for the electrons and the drift-diffusion equations for the holes. The electric circuit is modeled by the network equations from modified nodal analysis. The coupling is realized by the node potentials providing the voltages applied to the semiconductor devices and the output device currents for the network model. The resulting partial differential-algebraic system is discretized in time by the 2-stage backward difference formula and in space by a mixed-hybrid finite-element method using Marini-Pietra elements. A static condensation procedure is applied to the coupled system reducing the number of unknowns. Numerical simulations of a one-dimensional *pn*-junction diode with time-depending voltage and of a rectifier circuit show the heating of the electrons which allows to identify hot spots in the devices. Moreover, the choice of the boundary conditions for the electron density and energy density is numerically discussed.

Key words. Energy-transport equations, circuit equations, semiconductor devices, modified nodal analysis, mixed finite-element method, diode, Graetz bridge.

AMS subject classifications. 65L80, 65M60, 65N30, 82D37.

1. Introduction.

In industrial applications, complex semiconductor device models are usually substituted by circuits of basic network elements (resistors, capacitors, inductors, voltage and current sources) resulting in simpler so-called compact models. Such a strategy was advantageous up to now since integrated circuit simulations were possible without computationally expensive device simulations. Parasitic effects and high frequencies in the circuits, however, require to take into account a very large number of basic elements and to adjust carefully a large number of parameters in order to achieve the required accuracy. Moreover, device heating and hot spots cannot be easily modeled by this approach.

Therefore, it is preferable to model those semiconductor devices which are critical for the parasitic effects by semiconductor transport equations. Since structural information about the resulting device–circuit equations was missing for a long time, the first approaches to couple circuits and devices were based on an extension of existing device simulators by more complex boundary conditions [35, 39] or the combination of device simulators with circuit simulators as a "black box" solver [15]. Both approaches, however, are not suitable for complex circuits in the high-frequency domain. In this work, we follow an approach that includes the device model into the network equations directly. As the device model is described by partial differential equations and the network equations are given by differential-algebraic equations (DAE), this results in a coupled system of *partial differential-algebraic equations (PDAE)*.

The mathematical analysis and numerical approximation of coupled network and

*The authors acknowledge partial support from the German Federal Ministry of Education and Research (BMBF), grant 03JUNAVN, and from the bilateral DAAD-Vigoni Program. This research is part of the ESF program "Global and geometrical aspects of nonlinear partial differential equations (GLOBAL)". The authors thank Prof. Caren Tischendorf (University of Köln) and Dr. Uwe Feldmann (Qimonda, Munich) for fruitful discussions.

†Institut für Mathematik, Universität Mainz, Staudingerweg 9, 55099 Mainz, Germany; e-mail: {brunk,juengel}@mathematik.uni-mainz.de.

‡Institut für Analysis und Scientific Computing, Technische Universität Wien, Wiedner Hauptstr. 8-10, 1040 Wien, Austria; e-mail: juengel@anum.tuwien.ac.at.

device equations were studied only recently. The first mathematical results were obtained in [18, 20] where a semiconductor device was coupled to a simple circuit in such a way that the currents entering the device can be expressed by a function of the applied voltage. In this case, the network is treated only as a special boundary condition for the semiconductor. This approach fails for integrated circuits. A network containing uniform lossy transmission lines was investigated in [21]. The resulting model becomes a PDAE system, but with partial differential equations of hyperbolic type. An electro-thermal problem coupling the network model with a heat equation containing a local dissipative power term was numerically solved in [4].

Later, networks with semiconductor devices described by the drift-diffusion equations were studied. An existence analysis containing the drift-diffusion model was developed in [1, 2]. For a reliable and efficient numerical simulation, it is important to know the index of the PDAE system consisting of the network and drift-diffusion equations. It has been shown in [46] that the coupled circuit is of (tractability) index one if and only if the network(s) without the semiconductors satisfy some topological conditions, i.e., if they contain neither CV-loops nor LI-cutsets. Here, a loop consisting of capacitors and voltage sources only is called a CV-loop, whereas a cutset containing inductors and current sources only is called an LI-cutset. In [47] it was proved that the index of the coupled system is at most two under weak conditions on the circuit (local passivity, no shortcuts). Moreover, the index of the coupled system is two if and only if the circuit contains LI-cutsets or CVS-loops (loops of capacitors, voltage sources, and semiconductors) with at least one voltage source or one semiconductor device. The same results were obtained in [42] for the discretized drift-diffusion equations. A sensitivity analysis generalizing the DAE index for finite systems to infinite ones was presented in [7] and applied to the coupled PDAE system. It was shown that the system is of index one if the voltages applied to the semiconductors are low and the network without the semiconductors is of index one.

In this paper, we couple and simulate the network equations with the energy-transport model for semiconductors for the first time. Compared to the coupling with the drift-diffusion equations, we are able to calculate the electron temperature in the devices. The energy-transport model can be derived from the semiconductor Boltzmann equation in the diffusion limit under the assumption of dominant electron-electron scattering [5]. It consists of the conservation laws for the electron density and the electron energy density with constitutive relations for the particle and energy current densities, coupled to the Poisson equation for the electric potential. Mathematically, the energy-transport equations (without the Poisson equation) constitute a parabolic cross-diffusion system in the entropic variables [14]. The system can be written in a drift-diffusion-type formulation, which allows for an efficient numerical approximation [13].

The energy-transport model is discretized by mixed-hybrid finite elements of Marini-Pietra type [32, 33]. The one-dimensional equations are considered in order to test the coupling and to achieve a fast algorithm required by our industrial partner. For two-dimensional simulations of the energy-transport model (without any coupling to circuits), we refer to [23, 24]. Marini-Pietra finite elements instead of standard Raviart-Thomas elements are employed since this guarantees the M-matrix property of the global stiffness matrix, even in the presence of zeroth-order terms. Hence, the positivity of the particle densities is guaranteed. For the bipolar devices considered in this paper, we model the flow of the positively charged holes by the drift-diffusion equations which are also approximated by mixed Marini-Pietra finite

elements.

The network equations as well as the parabolic equations are discretized in time by the 2-stage backward difference formula (BDF2) since this scheme allows to maintain the M-matrix property. Then, the semi-discretized equations are approximated by the mixed finite-element method and static condensation is applied to reduce the number of variables (see section 3 for details). The final nonlinear discrete system is solved by Newton's method.

For large applied bias, we observe strong gradients of the temperature at the boundary. Employing Robin boundary conditions for the electron density and energy density instead of standard Dirichlet conditions allows to essentially eliminate the boundary layer. This is the first time that the energy-transport equations are numerically solved with Robin boundary conditions.

The paper is organized as follows. In section 2 we describe the circuit model using modified nodal analysis and the semiconductor device model employing the energy-transport equations. Moreover, the coupling of both models is explained. Section 3 is devoted to the numerical discretization of the circuit and semiconductor equations. In section 4 two circuits containing one-dimensional semiconductor devices are simulated, namely a *pn*-junction diode with time-depending applied voltage and a rectifier circuit with four *pn* diodes. The numerical results from the transient energy-transport equations are compared with those from the stationary energy-transport model and from the transient drift-diffusion equations. Finally, we conclude in section 5.

2. Modeling. In this section we explain the modeling of the electric circuits by modified nodal analysis and of the semiconductor devices using the energy-transport and drift-diffusion equations. Furthermore, the coupling of both models is made explicit.

2.1. Circuit modeling. The circuits considered in this paper are supposed to contain (ideal) resistors, capacitors, inductors, and voltage sources. In addition, we use ideal current sources, as they appear in proper compact models for semiconductor devices. Thus we can reduce these electric circuits by RCL-circuits (just containing resistors, capacitors, and inductors).

A well-established mathematical description of RCL-circuits is the modified nodal analysis. The basic tools are the Kirchhoff laws and the current-voltage characteristics of the basic elements. In order to accomplish the modified nodal analysis, the circuit is replaced by a directed graph with branches and nodes. Branch currents, branch voltages, and node potentials (without the mass node) are introduced as (time-dependent) variables. Then, the circuit can be characterized by the incidence matrix $A = (a_{jk})$ describing the node-to-branch relations and defined as

$$a_{jk} = \begin{cases} 1 & \text{if the branch } k \text{ leaves the node } j, \\ -1 & \text{if the branch } k \text{ enters the node } j, \\ 0 & \text{else.} \end{cases}$$

(see [48] for details on circuit topologies). The Kirchhoff current law expresses that the sum of all branch currents entering a node is equal to zero,

$$Ai = 0,$$

and the Kirchhoff voltage law means that the sum of all branch voltages in a loop vanishes, which can be expressed here as

$$v = A^\top e,$$

where i, v, and e are the vectors of branch currents, branch voltages, and node potentials, respectively. The current-voltage characteristics for the basic elements can be given as

$$i_R = g(v_R), \quad i_C = \frac{dq}{dt}(v_C), \quad v_L = \frac{d\Phi}{dt}(i_L),$$

where g denotes the conductivity of the resistor, q the charge of the capacitor, and Φ the flux of the inductor. Moreover, i_α and v_α with $\alpha = R$, C, L, are the branch current vectors and branch voltage vectors for, respectively, all resistors, capacitors, and inductors. The network branches are numbered in such a way that the incidence matrix forms a block matrix with blocks describing the different types of network elements, i.e., A consists of the block matrices A_R, A_C, A_L, A_i, and A_v, where the index indicates the resistive, capacitive, inductive, current source, and voltage source branches, respectively.

Denoting by $i_s = i_s(t)$ and $v_s = v_s(t)$ the given input functions for the current and voltage sources, respectively, and replacing the branch currents in the Kirchhoff current law by the current-voltage characteristics and the branch voltages by node potentials using the Kirchhoff voltage law, we obtain the system in the charge-oriented modified nodal analysis approach [48],

$$A_C\frac{dq}{dt}(A_C^\top e) + A_R g(A_R^\top e) + A_L i_L + A_v i_v = -A_i i_s, \tag{2.1}$$

$$\frac{d\Phi}{dt}(i_L) - A_L^\top e = 0, \tag{2.2}$$

$$A_v^\top e = v_s \tag{2.3}$$

for the unknowns $e(t)$, $i_L(t)$, and $i_v(t)$. Equation (2.1) is the Kirchhoff current law for the complete circuit, where the current-voltage relations for the resistors and capacitors have been included. Equation (2.2) decribes the voltage-current characteristic for the inductors, and (2.3) determines the node potentials adjacent to the given voltage sources.

Equations (2.1)-(2.3) represent a system of differential-algebraic equations (DAE) with a properly stated leading term [30, 31] if the matrices $C(v,t) = (\partial q/\partial v)(v,t)$ and $L(i,t) = (\partial\Phi/\partial i)(i,t)$ are positive definite for all arguments v, i, and t. Under the assumptions that the matrices C, L, and $G = \partial g/\partial v$ are positive definite and that the circuit does neither contain loops of voltage sources only nor cutsets of current sources only, it is proved in [46, 48] that the (tractability) index of the DAE system is at most two. Furthermore, if the circuit does neither contain LI-cutsets nor CV-loops with at least one voltage source (see the introduction) then the index is at most one.

2.2. Semiconductor device modeling. In the semiconductor device, we assume that the electron flow can be described by the energy-transport equations. They consist of the (scaled) conservation laws for the particle density n and energy density w,

$$\partial_t n - \mathrm{div} J_n = -R(n,p), \tag{2.4}$$

$$\partial_t w - \mathrm{div} J_w = -J_n\cdot\nabla V + W(n,T) - \frac{3}{2}TR(n,p), \tag{2.5}$$

together with (scaled) constitutive relations for the particle current J_n and energy current density J_w,

$$J_n = \mu_n\Big(\nabla n - \frac{n}{T}\nabla V\Big), \quad J_w = \frac{3}{2}\mu_n(\nabla(nT) - n\nabla V), \tag{2.6}$$

coupled self-consistently to the Poisson equation for the electric potential V,

$$\lambda^2 \Delta V = n - p - C(x). \tag{2.7}$$

Here, the electron temperature T is defined via the relation $w = \frac{3}{2} nT$, p denotes the hole density determined by the drift-diffusion equations

$$\partial_t p + \mathrm{div} J_p = -R(n,p), \quad J_p = -\mu_p(\nabla p + p \nabla V), \tag{2.8}$$

and the function $C(x)$ models fixed charged background ions in the semiconductor crystal (doping profile). The physical parameters are the (scaled) electron and hole mobilities μ_n and μ_p and the Debye length λ, given by

$$\lambda^2 = \frac{\varepsilon_s U_T}{q C_m L},$$

where ε_s is the permittivity constant, $U_T = k_B T_L / q$ with the Boltzmann constant k_B, the lattice temperature T_L and the elementary charge q denotes the thermal voltage, C_m is the maximal doping value, and L is the device diameter. The equations (2.4)-(2.8) are solved in the bounded domain Ω. The function

$$W(n,T) = -\frac{3}{2} \frac{n(T - T_L)}{\tau_0}$$

with the (scaled) energy relaxation time τ_0 and the lattice temperature $T_L = 1$ describes the energy relaxation to the equilibrium energy, and

$$R(n,p) = \frac{np - n_i^2}{\tau_p(n + n_i) + \tau_n(p + n_i)} \tag{2.9}$$

models recombination-generation processes with the (scaled) intrinsic density n_i and the material-depending electron and hole lifetimes τ_n and τ_p, respectively.

We have used the following scaling. The densities n, p, n_i, and C are scaled by the maximal doping concentration $C_m = \max |C(x)|$; the temperature is scaled by the lattice temperature (usually, 300 K); the electric potential by the thermal voltage U_T; the mobilities μ_n and μ_p by $\bar{\mu} = \max\{\mu_n, \mu_p\}$; and finally, the relaxation time τ_0 and the lifetimes τ_n, τ_p by $t_0 = L^2/(U_T \bar{\mu})$. For notational convenience, we have not renamed the scaled quantities.

For the model equations (2.4)-(2.8) we need to impose appropriate initial and boundary conditions. We prescribe the initial conditions for the particle densities and the temperature

$$n(\cdot,0) = n_I, \quad p(\cdot,0) = p_I, \quad T(\cdot,0) = T_I \quad \text{on } \partial\Omega. \tag{2.10}$$

The device boundary is assumed to split into two parts, the union of Ohmic contacts Γ_D and the union of insulating boundary segments Γ_N, where $\partial\Omega = \Gamma_D \cup \Gamma_N$. Although we will present later spatial one-dimensional simulations, we give the boundary conditions for the multidimensional situation. On the insulating parts, it is assumed that the normal components of the current densities and of the electric field vanish,

$$J_n \cdot \nu = J_p \cdot \nu = J_w \cdot \nu = \nabla V \cdot \nu = 0 \quad \text{on } \Gamma_N, \ t > 0. \tag{2.11}$$

At the contacts, the temperature, the electric potential, and the particle densities are assumed to be known. The electric potential equals the sum of the applied voltage U and the so-called built-in potential $V_{\rm bi}$,

$$V = U + V_{\rm bi} \quad \text{on } \Gamma_D,\ t > 0. \tag{2.12}$$

The built-in potential is the potential in the device in thermal equilibrium,

$$V_{\rm bi} = \operatorname{arsinh}\Big(\frac{C}{2n_i}\Big).$$

The temperature is supposed to be equal to the (scaled) lattice temperature at the contacts:

$$T = 1 \quad \text{on } \Gamma_D,\ t > 0. \tag{2.13}$$

The boundary conditions for the particle densities are derived under the assumptions of charge neutrality, $n - p - C(x) = 0$, and thermal equilibrium, $np = n_i^2$. Solving these equations for n and p gives

$$n = \frac{1}{2}\Big(C + \sqrt{C^2 + 4n_i^2}\Big), \quad p = \frac{1}{2}\Big(-C + \sqrt{C^2 + 4n_i^2}\Big) \quad \text{on } \Gamma_D. \tag{2.14}$$

We will show in section 4 that the Dirichlet boundary conditions for the particle densities and the temperature may lead, for large applied voltages, to strong boundary layers. Therefore, we will also employ Robin boundary conditions for comparison (see section 4).

Energy-transport models have been used by engineers for more than 40 years to describe thermal effects in semiconductor devices [44], mostly with phenomenological transport coefficients. In the physical literature, these models have been usually derived from hydrodynamic equations by neglecting certain convection terms (see [40] and references therein). Another approach is to derive the energy-transport models from the semiconductor Boltzmann equation by using a Hilbert expansion method under the assumptions of nondegenerate Boltzmann statistics and dominant electron-electron and elastic collisions [5]. Depending on the conditions on the microscopic relaxation time, various energy-transport models can be derived [13]. Here, we employ the model of [11] which is also used in the simulations of [23, 24].

The numerical discretization of energy-transport models has been investigated in the physical literature for quite some time [11, 16, 43]. Mathematicians started to pay attention to these models in the 1990s, using essentially non-oscillatory (ENO) schemes [25], finite-difference methods [17, 38], mixed finite-volume schemes [8], or mixed finite-element methods [23, 24, 27, 34] (also see [10] for an overview).

In this paper, we will use as in [13] the mixed finite-element method applied to the drift-diffusion-like formulation of the energy-transport model since this method allows for a good approximation of the current densities (see, e.g. [3, 10]). For this, we define the variables $g_1 = \mu_n n$ and $g_2 = \frac{3}{2}\mu_n nT$ and write (2.4)-(2.6) as

$$\begin{aligned}
&\mu_n^{-1}\partial_t g_1 - \operatorname{div} J_n = -R(n,p),\\
&\mu_n^{-1}\partial_t g_2 - \operatorname{div} J_w = -J_n\cdot\nabla V + W(n,T) - \frac{3}{2}TR(n,p)
\end{aligned}$$

with the current densities

$$J_n = \nabla g_1 - \frac{g_1}{T}\nabla V, \quad J_w = \nabla g_2 - \frac{g_2}{T}\nabla V, \tag{2.15}$$

where the temperature is now given by $T = 2g_2/3g_1$. This corresponds (up to a sign) to the drift-diffusion equations (2.8), where p is replaced by g_1 or g_2, $T = 1$, and the right-hand side is different. The initial and boundary conditions for g_1, g_2, and V now follow directly from (2.10)-(2.14).

2.3. Coupling. The coupling is realized on the one hand by the semiconductor current density from the energy-transport and drift-diffusion equations, which needs to be included in the Kirchhoff current law (2.1), and on the other hand by the potentials of the circuit nodes adjacent to the semiconductor device, defining the boundary condition for the electric potential in the device.

First, we consider the semiconductor current density which consists of three parts, the electron current J_n, the hole current J_p, and the displacement current J_d caused by the electric potential and given by $J_d = -\lambda^2 \partial_t \nabla V$. The total current density $J_{\rm tot}$ is then given by

$$J_{\rm tot} = J_n + J_p + J_d.$$

The displacement current guarantees charge conservation. Indeed, differentiating the Poisson equation (2.7) with respect to time and replacing the time derivatives of the particle densities by (2.4) and (2.8), we obtain

$$\mathrm{div} J_{\rm tot} = \mathrm{div}(J_n + J_p) - \partial_t(n - p) = 0.$$

The current leaving the semiconductor device at terminal k, corresponding to the Dirichlet boundary part Γ_k, is defined by

$$j_k = \int_{\Gamma_k} J_{\rm tot} \cdot \nu \, ds.$$

Clearly, due to charge conservation, the current through one terminal can be computed by the negative sum of the currents through all other terminals. Therefore, it is possible to choose one terminal (usually the bulk terminal) as the reference terminal. We denote by j_S the vector of all terminal currents except the current corresponding to the reference terminal. In the one-dimensional case, there remains only one terminal, and the current through the terminal at $x = 0$ is given by

$$j_S(t) = J_n(0,t) + J_p(0,t) - \lambda^2 \partial_t V_x(0,t).$$

Now, we define the semiconductor incidence matrix A_S by its elements

$$a_{ik} = \begin{cases} 1 & \text{if the current } j_k \text{ enters the circuit node } i, \\ -1 & \text{if the reference terminal is connected to the node } i, \\ 0 & \text{else.} \end{cases}$$

Including the row for the mass node, each column of A_S has exactly one entry 1 and one entry -1. Therefore, it is of the same form as the other incidence matrices introduced in section 2.1 and can be added to the Kirchhoff current law (2.1), leading to

$$A_C \frac{dq}{dt}(A_C^\top e) + A_R g(A_R^\top e) + A_L i_L + A_v i_v + A_S j_S = -A_i i_s.$$

Notice that this procedure extends easily to the case of several semiconductors. In this situation, we need to choose one reference terminal for each semiconductor device

and to follow the above procedure for each device. We notice that the scaling of time in the semiconductor model also changes the time variable in the above DAE system, for instance $t = t_0 t_s$, where t_0 is the scaling factor and t_s is the scaled time, and the time derivative d/dt has to be replaced by $t_0^{-1}(d/dt_s)$.

The second part of the coupling is described via the boundary conditions for the electric potential in the semiconductor device. On the terminal k, we have

$$V(t) = e_i(t) + V_{\rm bi} \quad \text{on } \Gamma_k,$$

if the terminal k of the device is connected to the circuit node i, where e_i denotes the potential at the circuit node i.

We summarize the complete coupled system with one-dimensional semiconductor equations. The network equations are given by

$$\begin{aligned} A_C\frac{dq}{dt}(A_C^\top e) + A_R g(A_R^\top e) + A_L i_L + A_v i_v + A_S j_S &= -A_i i_s, \\ \frac{d\Phi}{dt}(i_L) - A_L^\top e &= 0, \\ A_v^\top e &= v_s, \end{aligned}$$

the current j_S is defined by

$$j_{d,S} - \lambda^2 V_x = 0, \quad j_S - (J_n + J_p - \partial_t j_{d,S}) = 0, \tag{2.16}$$

the semiconductor model reads as

$$\begin{aligned} &\mu_n^{-1}\partial_t g_1 - J_{n,x} = -R, \quad \lambda^2 V_{xx} = \mu_n^{-1} g_1 - p - C(x), \\ &\mu_n^{-1}\partial_t g_2 - J_{w,x} = -J_n V_x + W - \frac{3}{2}TR, \quad \partial_t p + J_{p,x} = -R, \end{aligned}$$

together with the current relations

$$J_n = g_{1,x} - \frac{g_1}{T}V_x, \quad J_w = g_{2,x} - \frac{g_2}{T}V_x, \quad J_p = -\mu_p\left(p_x + pV_x\right).$$

The boundary conditions for the potential are

$$V(0,t) = e_i + V_{\rm bi}(0), \quad V(1,t) = e_j + V_{\rm bi}(1)$$

for appropriate nodes e_i and e_j. The remaining boundary conditions for g_1, g_2, and T are given by

$$\begin{aligned} n(x,t) &= \frac{1}{2}\Big(C(x) + \sqrt{C(x)^2 + 4n_i^2}\Big), \quad T(x,t) = T_L, \\ p(x,t) &= \frac{1}{2}\Big(-C(x) + \sqrt{C(x)^2 + 4n_i^2}\Big) \quad \text{at } x = 0, 1. \end{aligned}$$

For the choice of initial conditions, we refer to section 4.

The equations above form a system of partial differential-algebraic equations. We have already mentioned in the introduction that the partial differential-algebraic equations resulting from a coupled circuit with the drift-diffusion equations have at most index 2 and that they have index 1 under some topological assumptions [6, 47]. No analytical result is available for the coupled system consisting of the circuit and energy-transport equations. However, we conjecture that the index of this system is also at most two.

3. Numerical approximation.

3.1. Numerical integration of DAEs. For the numerical integration of differential-algebraic equations (DAEs) we can employ Runge-Kutta methods or backward difference formulas (BDF). For Runge-Kutta methods applied to DAEs we refer to [22], for instance. Only implicit Runge-Kutta schemes are feasible for DAEs, and stiffly accurate methods provide the best properties. For instance, stiffly accurate methods for index-1 DAEs have the same convergence order as in the case of the numerical integration of explicit ordinary differential equations. For other Runge-Kutta methods, order reduction in the algebraic part down to the stage order q occurs. For stiffly accurate methods for index-2 DAEs, an order reduction in the differential and algebraic part down to the order $q+1$ can be observed. For other methods, even stronger order reduction may occur.

Concerning BDF methods, k-step BDF (with $k < 7$) for index-1 DAEs are feasible for sufficiently small time steps, and they are convergent with the same order as in the case of explicit ordinary differential equations [29]. The numerical integration of index-2 DAEs with BDF is studied in [9, 22]. In [45], quasilinear index-2 DAEs, as they occur in circuit simulation, were examined. It has been shown that k-step BDF for $k < 7$ are feasible and weakly instable under suitable assumptions. The convergence order is the same as in the case of explicit ordinary differential equations.

In the previous subsection, we made the conjecture, based on coupled drift-diffusion and network equations, that the index of the partial differential-algebraic system derived in section 2.3 is not larger than two. Therefore, we employ the 2-step BDF, defined by

$$\partial_t g(t_m) \approx \frac{1}{2\triangle t}(3g^{(m+1)} - 4g^{(m)} + g^{(m-1)}), \tag{3.1}$$

where $g^{(k)}$ approximates $g(\cdot, t_k)$, $t_k = k\triangle t$. We found that on the one hand, simple methods like the implicit Euler scheme have a too strong damping effect. On the other hand, methods like Radau IIa are not suitable since the stiffness matrix coming from the finite-element discretization of the semiconductor equations does not provide an M-matrix after static condensation (see below for details). Using the 2-step BDF allows to keep the M-matrix property provided by the finite-element scheme. Furthermore, higher-order schemes are not appropriate here, since the input signals may be discontinuous.

3.2. Numerical discretization of the energy-transport equations. The semiconductor equations are discretized in time by the 2-step BDF (see section 3.1) and in space by a mixed-hybrid finite-element scheme. The Poisson equation is discretized by a standard P_1 finite-element method. Thus, the discrete electric potential is piecewise linear and the approximation of the electric field $-V_x$ is piecewise constant. In the following we only describe the discretization of the electron and energy equation, since the discretization of the hole equation is similar.

The recombination-generation term (2.9) is treated semi-linearly. More precisely, we employ in the denominator the values of the particle densities from the former time step, whereas in the enumerator, one of the particle densities is fixed (using again the values of the previous time step). In this way, the recombination-generation term becomes, in each iteration step, linear. For given V, T, and p and $\widetilde{g}_1$ and $\widetilde{J}_n$ from the previous time step, we can thus express the continuity equations as

$$\mu_n^{-1}\partial_t g_j - J_{j,x} + \bar{\sigma}_j g_j = \bar{f}_j, \quad j = 1, 2,$$

where the current densities $J_1 = J_n$ and $J_2 = J_w$ are given by (2.15) and

$$\bar{\sigma}_1 = \frac{\mu_n^{-1} p}{\tau_p(\mu_n^{-1}\widetilde{g}_1 + n_i) + \tau_n(p + n_i)}, \quad \bar{\sigma}_2 = \frac{3}{2}T\bar{\sigma}_1 + (\mu_n\tau_0)^{-1},$$
$$\bar{f}_1 = \frac{n_i^2}{\tau_p(\mu_n^{-1}\widetilde{g}_1 + n_i) + \tau_n(p + n_i)}, \quad \bar{f}_2 = \frac{3}{2}T\bar{f}_1 - \widetilde{J}_n V_x + \frac{3}{2}(\mu_n\tau_0)^{-1}T_L\widetilde{g}_1.$$

After time discretization with the 2-step BDF (3.1) we obtain at time $t_{m+1} = (m+1)\triangle t$

$$-J_{j,x} + \sigma_j g_j = f_j, \quad J_j = g_{j,x} - \frac{g_j}{T}V_x, \quad j = 1, 2, \tag{3.2}$$

where

$$\sigma_j = \bar{\sigma}_j + \frac{3}{2}(\mu_n\triangle t)^{-1}g_j, \quad f_j = \bar{f}_j + 2(\mu_n\triangle t)^{-1}g_j^{(m)} - \frac{1}{2}(\mu_n\triangle t)^{-1}g_j^{(m-1)}$$

and $g_j^{(m)}$ and $g_j^{(m-1)}$ are the values of g_j from the previous time steps.

In the following we explain the spatial discretization of (3.2) using mixed finite elements. In the case $\sigma_j = 0$, the use of the lowest-order Raviart-Thomas elements [37] guarantees that the resulting stiffness matrix is an M-matrix. This provides a positivity-preserving numerical scheme, i.e., the discrete particle densities stay positive if they are positive initially and on the boundary. Unfortunately, this property generally does not hold in the presence of the zeroth-order term $\sigma_i g_i$. Marini and Pietra [33] have developed finite elements which guarantee the M-matrix property even with zeroth-order terms. They have been successfully applied to the energy-transport equations in one and two space dimensions [13, 23, 24].

We consider (3.2) in the interval $(0, 1)$ with Dirichlet boundary conditions (see section 2.3) and with Robin boundary conditions (see section 4). For convenience, we omit the index j in (3.2). We introduce the uniform mesh $x_i = ih$, $i = 0, \ldots, N$, where $N \in \mathbb{N}$ and $h = 1/N$. In order to deal with the convection dominance due to high electric fields, we use exponential fitting. Assume in the following that the temperature is given by a piecewise constant function $\overline{T}$ (see (3.6) for the definition of $\overline{T}$) and that the electric potential V is a given piecewise linear function. Then we define a local Slotboom variable by $y = \exp(-V/\overline{T})g$ in each subinterval $I_i = (x_{i-1}, x_i)$. Equation (3.2) can be written as

$$e^{-V/\overline{T}}J - y_x = 0, \quad -J_x + \sigma e^{V/\overline{T}}y = f.$$

The ansatz space for the current density J consists of piecewise polynomials of the form $\psi_i(x) = a_i + b_i P_i(x)$ on each I_i with constants a_i, b_i and second-order polynomials $P_i(x)$ which are defined as follows. Let $P(x)$ be the unique second-order polynomial satisfying $\int_0^1 P(x)dx = 0$, $P(0) = 0$, and $P(1) = 1$. Then $P(x) = 3x^2 - 2x$. We define $P_i(x)$ (depending on V) by

$$P_i(x) = -P\Big(\frac{x_i - x}{h}\Big) \quad \text{for } i_{\min} = i - 1,$$
$$P_i(x) = P\Big(\frac{x - x_{i-1}}{h}\Big) \quad \text{for } i_{\min} = i,$$

where $i_{\min}$ is the boundary node of I_i at which the potential attains its minimum. Notice that the minimum is always attained at the boundary since V is linear on I_i. If V is constant in I_i, we define $P_i(x) = P((x - x_{i-1})/h)$.

Now we introduce the finite-dimensional spaces:

$$V_h = \{\psi \in L^2(0,1) : \psi(x) = a_i + b_i P_i(x) \text{ in } I_i,\ i = 1,\dots,N\},$$
$$W_h = \{\phi \in L^2(0,1) : \phi \text{ is constant in } I_i,\ i = 1,\dots,N\},$$
$$\Gamma_{h,\xi} = \{q \text{ is defined at the nodes } x_0,\dots,x_N,\ q(x_0) = \xi(0),\ q(x_N) = \xi(1)\}.$$

The mixed-hybrid finite-element approximation of (3.2) is as follows. Find $J_h \in V_h$, $\bar{g}_h \in W_h$, and $g_h \in \Gamma_{h,g_D}$ such that

$$\sum_{i=1}^N \Big(\int_{I_i} Q_i J_h \psi dx + \int_{I_i} S_i \bar{g}_h \psi_x dx - \Big[e^{-V/\overline{T}_i} g_h \psi \Big]_{x_{i-1}}^{x_i} \Big) = 0, \tag{3.3}$$

$$\sum_{i=1}^N \Big(-\int_{I_i} J_{h,x} \phi dx + \int_{I_i} \sigma \bar{g}_h \phi dx \Big) = \sum_{i=1}^N \int_{I_i} f \phi dx, \tag{3.4}$$

$$\sum_{i=1}^N \big[q J_h \big]_{x_{i-1}}^{x_i} = 0 \tag{3.5}$$

for all $\psi \in V_h$, $\phi \in W_h$, and $q \in \Gamma_{h,0}$, where g_D denotes the Dirichlet boundary values of g, and

$$Q_i = \frac{1}{h} \int_{I_i} e^{-V(x)/\overline{T}_i} dx, \quad S_i = e^{-V_{\min}/\overline{T}_i}, \quad i = 1,\dots,N,$$

are introduced in order to treat accurately large gradients of the potential [33]. Here, $V_{\min}$ denotes the minimal value of V on I_i. Equation (3.3) is the weak formulation of the second equation in (3.2), together with the inverse of the Slotboom transformation. Notice that the discrete inverse transformation is not the same for the variables $\bar{g}_h$ and g_h. Equation (3.4) is the discrete weak version of the first equation in (3.2). The third equation (3.5) implies the continuity of J_h at the nodes. Clearly, in the case of Robin boundary conditions, these equations have to be modified appropriately.

The additional variables J_h and $\bar{g}_h$ can be eliminated by static condensation. For this, we write the weak formulation in matrix-vector notation for the vectors of nodal values similarly as in [23]:

$$\begin{pmatrix} A & \widetilde{B}^\top & -\widetilde{C}^\top \\ -B & D & 0 \\ C & 0 & 0 \end{pmatrix} \begin{pmatrix} J_h \\ \bar{g}_h \\ g_h \end{pmatrix} = \begin{pmatrix} 0 \\ F \\ 0 \end{pmatrix}.$$

The matrices $A \in \mathbb{R}^{2N\times 2N}$, $B \in \mathbb{R}^{N\times 2N}$, $C \in \mathbb{R}^{(N-1)\times 2N}$, and $D \in \mathbb{R}^{N\times N}$ are given by the corresponding elementary matrices associated with the interval I_i, denoted by the superscript i:

$$A_{jk}^i = Q_i \int_{I_i} \psi_j \psi_k dx, \qquad B_{jk}^i = \int_{I_i} \phi_j \psi_{k,x} dx,$$
$$C_{jk}^i = \big[q_j \psi_k \big]_{x_{i-1}}^{x_i}, \qquad D_{jk}^i = \int_{I_i} \sigma \phi_j \phi_k dx,$$

where ψ_k, ϕ_k, and q_k are the canonical basis functions of the corresponding spaces. Furthermore, the matrices $\widetilde{B}$ and $\widetilde{C}$ are given by the elementary matrices

$$\widetilde{B}^i = S_i B^i, \quad \widetilde{C}_{jk}^i = \big[e^{-V_j/\overline{T}_i} q_j \psi_k \big]_{x_{i-1}}^{x_i},$$

and the right-hand side F represents the integral on the right-hand side of (3.4).

Now, static condensation as in [23] can be applied. As the matrix A has a diagonal structure, it can be easily inverted, which allows to eliminate J_h. A similar argument for $BA^{-1}\widetilde{B}^\top + D$ allows to eliminate g_h. This leads to the system

$$M\bar{g}_h = G.$$

The stiffness matrix M has a tridiagonal structure with diagonal elements

$$M_{ii} = \frac{1}{h}\Big(N_{i+1} + \frac{V_{i+1}-V_i}{2\overline{T}_{i+1}} + N_i - \frac{V_i - V_{i-1}}{2\overline{T}_i}\Big) + \frac{h\sigma_i}{\gamma_i\sigma_i+1}P_i(x_i) - \frac{h\sigma_{i+1}}{\gamma_{i+1}\sigma_{i+1}+1}P_{i+1}(x_i),$$

where

$$N_i = \frac{V_i - V_{i-1}}{2\overline{T}_i}\coth\frac{V_i-V_{i-1}}{2\overline{T}_i}, \quad \gamma_i = \frac{2}{15}h^2Q_ie^{V_{\min}/\overline{T}_i},$$

$V_i = V(x_i)$, σ_i is the restriction of the piecewise constant function σ to I_i, and the elements on the secondary diagonals are

$$M_{i,i+1} = \frac{1}{h}\Big(-N_{i+1} + \frac{V_{i+1}-V_i}{2\overline{T}_{i+1}}\Big), \quad M_{i+1,i} = \frac{1}{h}\Big(-N_i - \frac{V_i-V_{i-1}}{2\overline{T}_i}\Big).$$

It is not difficult to see that M is an M-matrix. In particular, it holds $M_{ij} \le 0$ for all $i \ne j$. In view of the construction of the polynomial P_i, it holds either $P_i(x_i) = 1$ and $P_i(x_{i-1}) = 0$ or $P_i(x_i) = 0$ and $P_i(x_{i-1}) = -1$. Thus $M_{ii} \ge 0$.

The components of the vector G are given by

$$G_i = \frac{hf_i}{\gamma_i\sigma_i+1}P_i(x_i) - \frac{hf_{i+1}}{\gamma_{i+1}\sigma_{i+1}+1}P_{i+1}(x_{i+1}),$$

where f_i denotes the restriction of the piecewise constant function f (see (3.4)) to I_i. Thus, for nonnegative f, also G is nonnegative. Since M is an M-matrix, this shows the nonnegativity of the solution. For the equation for the particle densities, a nonnegative right-hand side f can be achieved by adjusting the size of the time step. We cannot guarantee generally nonnegativity of the right-hand side for the energy equation since the term $-J_nV_x$ may be negative and large. However, we observed that $-J_nV_x$ is negative in few cases only, and by adjusting the step size in space and time we always obtained positive solutions even for negative values of the right-hand side.

The eliminated variables $\bar{g}_h$ and J_h can be computed by the following relations:

$$\bar{g}_h^i = \frac{1}{\gamma_i\sigma_i+1}(g_h^{i_{\min}} + \gamma_i f_i),$$
$$J_h^i = N_i\frac{g_h^i - g_h^{i-1}}{h} - \frac{g_h^i + g_h^{i-1}}{2\overline{T}_i}\,\frac{V_i - V_{i-1}}{2\overline{T}_i} + \frac{h}{\gamma_i\sigma_i+1}(g_h^{i_{\min}}\sigma_i - f_i)P_i(x).$$

In order to complete the scheme, we still have to specify how the piecewise constant temperature $\overline{T}$ is defined. The temperature is implicitly defined in terms of g_1 and g_2, $T = 2g_2/3g_1$. Hence, we define

$$\overline{T}_i = \frac{1}{2}(T_i + T_{i-1}), \quad \text{where } T_i = \frac{2\bar{g}_{2,h}^i}{3\bar{g}_{1,h}^i}. \tag{3.6}$$

Parameter	Physical meaning	Numerical value
L_y	extension of device in y-direction	$6 \cdot 10^{-7}\,\mathrm{m}$
L_z	extension in z-direction	$10^{-6}\,\mathrm{m}$
q	elementary charge	$1.6 \cdot 10^{-19}\,\mathrm{As}$
ϵ_s	permittivity constant	$10^{-12}\,\mathrm{As/Vcm}$
U_T	thermal voltage at $T_L = 300K$	$0.026\,\mathrm{V}$
μ_n/μ_p	low-field carrier mobilities	$1500/450\,\mathrm{cm}^2/\mathrm{Vs}$
τ_n/τ_p	carrier lifetimes	$10^{-6}/10^{-5}\,\mathrm{s}$
n_i	intrinsic density	$10^{16}\,\mathrm{m}^{-3}$
τ_0	energy relaxation time	$4 \cdot 10^{-13}\,\mathrm{s}$

TABLE 4.1
Physical parameters for a silicon pn-junction diode.

For each time step, we have to solve a discrete nonlinear system corresponding to the discretized semiconductor equations and the network model. The Newton method is applied to the whole system. The temperature is updated during the Newton iterations only if

$$\|(g_{1,h}, g_{2,h}, p_h, V_h)_{\mathrm{new}} - (g_{1,h}, g_{2,h}, p_h, V_h)_{\mathrm{old}}\|_2 \le \max\{\varepsilon, c\|\overline{T}_{\mathrm{new}} - \overline{T}\|_2^d\},$$

where the parameters $\varepsilon = 10^{-7}$, $c = 0.01$, and $d = 0.08$ are chosen similarly as in [23]. For the first time step we apply the implicit Euler method (BDF1).

4. Numerical examples. In this section, we present the numerical results of two coupled circuit-semiconductor models, a *pn*-junction diode with time-depending voltage and a rectifier circuit (Graetz bridge) with four *pn* diodes.

4.1. A *pn* diode with time-depending voltage. We consider a silicon *pn*-junction with a time-depending voltage source. The diode is assumed to be homogeneous in the y- and the z-direction such that a one-dimensional approach is suitable. In order to unscale the current densities and to obtain a current (and not a current density), the size of the diode in the y- and z-direction are specified (see Table 4.1). The quasi one-dimensional diode consists of a p-doped region with length $L/2$ and minimal doping profile $-C_0$ and of a n-doped region with the same length and with a maximal doping of C_0. We have used the values $L = 0.1\,\mu\mathrm{m}$ or $L = 0.6\,\mu\mathrm{m}$ and $C_0 = 10^{22}\,\mathrm{m}^{-3}$ or $C_0 = 5 \cdot 10^{23}\,\mathrm{m}^{-3}$, respectively. The doping profile is slightly smoothed using the tanh function (see, e.g. [26]). The circuit operates with 1 GHz, i.e., the applied voltage equals $v(t) = U_0 \sin(2\pi\omega t)$ with maximal voltage $U_0 = 1.5\,\mathrm{V}$ and frequency $\omega = 10^9\,\mathrm{Hz}$. The physical parameters are collected in Table 4.1. We refer to [41] for more details about carrier life-times.

We have used a uniform spatial grid with 101 nodes and a uniform time step $\triangle t = 10^{-13}\,\mathrm{s}$. The time step is rather small; this can be explained by the fact that we need careful computations at the switching point when the voltage changes from forward to backward bias and vice versa. An adaptive time stepping procedure would certainly allow to choose larger time steps; we plan to implement this in the future.

Initially, the semiconductor device is assumed to be in thermal equilibrium, i.e., the total current of electrons and holes vanishes. Thus, the initial node potentials and the current densities are taken to be zero. The initial displacement current is then defined by $j_{d,S}(\cdot, 0) = \lambda^2 (V_{\mathrm{eq}})_x$, where V_{eq} denotes the thermal equilibrium potential

given by

$$\lambda^2(V_{\rm eq})_{xx} = e^{-V_{\rm eq}} - e^{V_{\rm eq}} - C(x), \quad V_{\rm eq}(0,\cdot) = V_{\rm bi}(0), \quad V_{\rm eq}(1,\cdot) = V_{\rm bi}(1).$$

Recall that $V_{\rm bi}$ is the built-in potential introduced in section 2.3. The definition of $j_{d,S}$ ensures that the first equation in (2.16) is fulfilled. Summarizing, the initial conditions read as follows:

$$\begin{array}{llll} e = 0, & i_V = 0, & j_S = 0, & j_{d,S} = \lambda^2(V_{\rm eq})_x, \\ g_1 = \mu_n n_{\rm eq}, & g_2 = \frac{3}{2}\mu_n n_{\rm eq}, & p = p_{\rm eq}, & V = V_{\rm eq}, \qquad T = 1, \end{array}$$

where $n_{\rm eq} = e^{-V_{\rm eq}}$ and $p_{\rm eq} = e^{V_{\rm eq}}$ are the thermal equilibrium particle densities. A computation shows that the initial conditions are consistent for the coupled system of PDAEs according to [28].

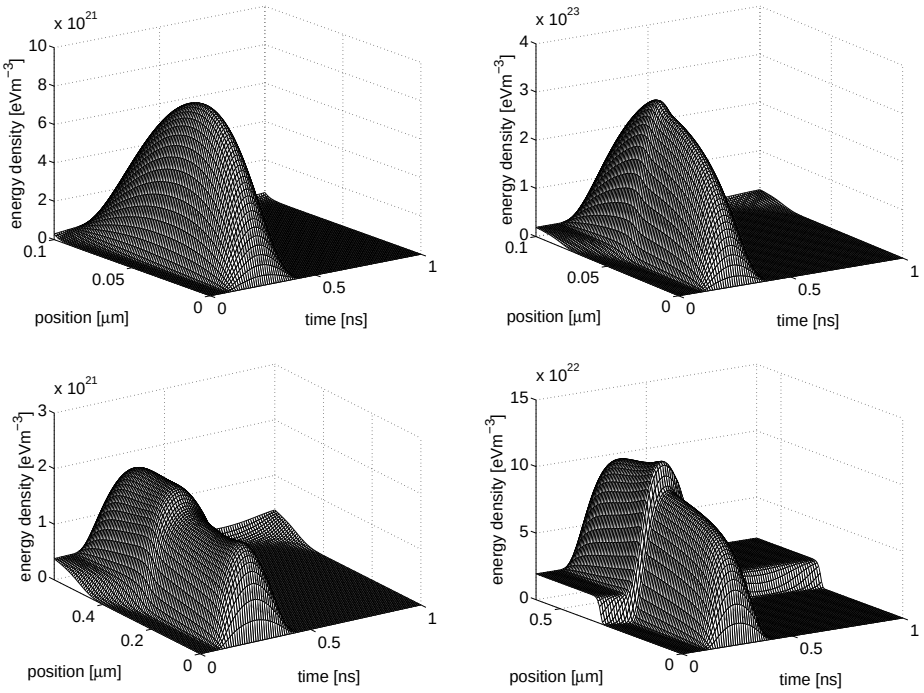

FIG. 4.1. *Energy density in a pn diode with lengths $L = 0.1\,\mu m$ (upper row), $L = 0.6\,\mu m$ (lower row) and maximal doping concentrations $C_0 = 10^{22}\,m^{-3}$ (left column), $C_0 = 5 \cdot 10^{23}\,m^{-3}$ (right column).*

In Figure 4.1 we present the electron density in *pn* diodes with different size L and different maximal doping concentrations C_0. We observe that a higher doping profile gives a larger energy density as it provides more (high-energetic) electrons in the device. The energy density also increases for smaller devices. This coincides with the experience that smaller devices heat up stronger than larger ones.

In Figure 4.2 (left) the electron temperature in a $0.6\,\mu$m diode with a maximal doping level of $10^{22}\,\mathrm{m}^{-3}$ at various times t_i (and corresponding voltages $v(t_i)$) is shown. We observe hot electrons in the n-region and close to the p-doped terminal. At the junction, cooling effects occur for moderate applied voltages. This thermoelectric

effect is well known in *pn* diodes and it has important implications for the device design in which heat management is needed (see, for instance, [36]).

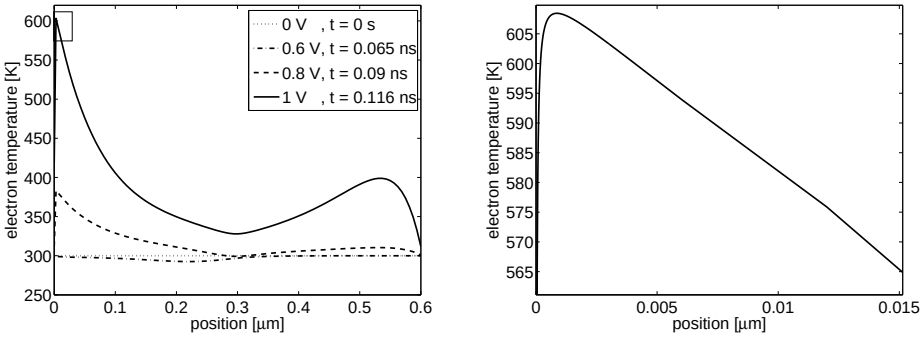

FIG. 4.2. *Left: Electron temperature in a* $0.6\,\mu m$ *diode with maximal doping level of* $10^{22}\ m^{-3}$ *for different times* t *and corresponding voltages* $v(t)$*. Right: Zoom for the bias* $v(t) = 1\ V$*.*

At the left p-doped terminal, there is a boundary layer which can be resolved only in high resolution (see Figure 4.2 right). In fact, there are boundary layers also for the electron density n as well as for the energy density $w = \frac{3}{2}nT$ (Figure 4.3). This seems to indicate that the use of Dirichlet boundary conditions for n and w (or, equivalently, for n and T) is not appropriate. For the drift-diffusion equations, Yamnahakki [50] has shown that Robin-type boundary conditions provide more accurate results than Dirichlet conditions. This can be explained roughly by the fact that the Robin-type conditions are derived in second order from the semiconductor Boltzmann equations, whereas the Dirichlet conditions are only of order one. Thus, a different choice of the boundary conditions might be more appropriate.

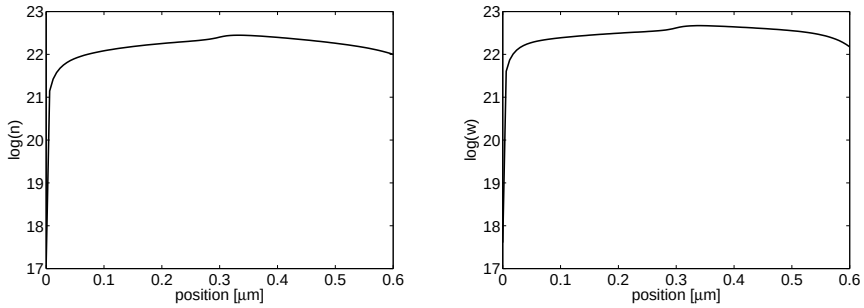

FIG. 4.3. *Logarithms of the electron density* n *(left) and energy density* w *(right) in a* $0.6\,\mu m$ *diode with a doping level of* $10^{22} m^{-3}$ *biased with* $1\ V$ *employing Dirichlet boundary conditions for* n *and* w*.*

As a first step, we propose the following Robin conditions,

$$n_x + \alpha(n - n_L) = 0, \quad w_x + \beta(w - w_L) = 0 \quad \text{at } x = 0, 1,$$

which interpolate between Dirichlet and Neumann conditions. Here, n_L is given by (2.14), $w_L = \frac{3}{2}n_L T_L$, T_L is the lattice temperature (300 K), and α and β are parameters. Notice that this implies Robin boundary conditions for T. Clearly, a

derivation of suitable higher-order boundary conditions from the Boltzmann equation in the energy-transport context would be necessary, but we postpone such an analysis to a future work. Furthermore, the boundary condition for the temperature should be compatible with the principle of local energy balance [49]. We do not analyze this property since we are more interested in the numerical solution of the coupled system of PDAEs.

Thanks to the new boundary conditions, the boundary layers for n and w disappear for an appropriate choice of the parameters α and β (Figure 4.4). The dependence of the temperature on these parameters is shown in Figure 4.5. These results indicate that the choice of the parameters is crucial for the temperature profile at the boundary. On the other hand, it can be seen that the current values are almost independent of the choice of α and β.

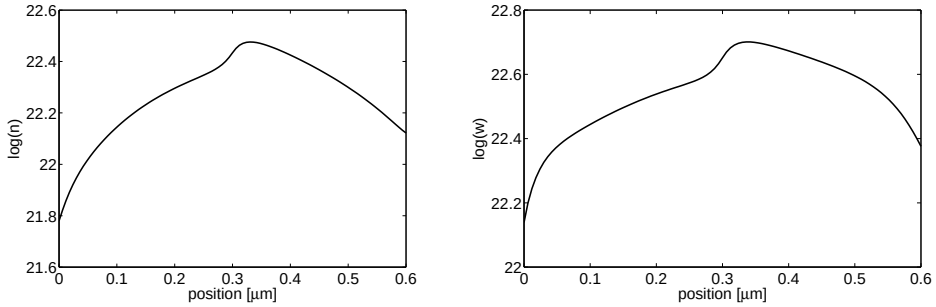

FIG. 4.4. *Logarithms of the electron density n (left) and energy density w (right) in a $0.6\,\mu m$ diode with a doping level of $10^{22}m^{-3}$ biased with $1\,V$ employing Robin boundary conditions for n and w and the parameters $\alpha = -10$, $\beta = -15$.*

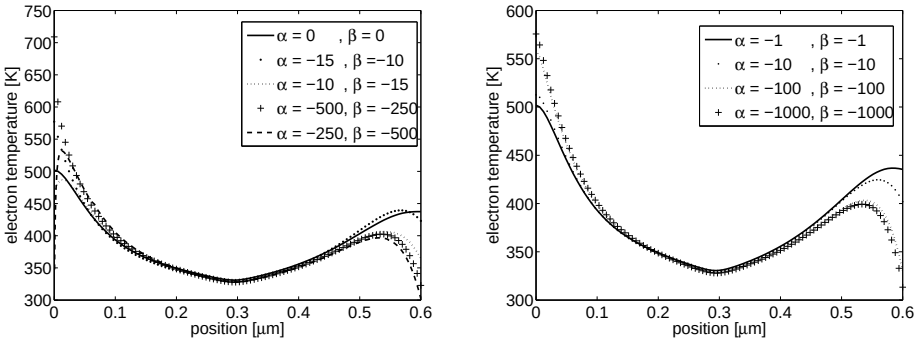

FIG. 4.5. *Electron temperature in a $0.6\,\mu m$ diode with a doping level of $10^{22}m^{-3}$ biased with $1\,V$ employing Robin boundary conditions for n and w for different choices of α and β.*

4.2. Rectifying circuit. The second example is concerned with a rectifying circuit containing four *pn* silicon diodes (Figure 4.6). Each of the diodes have the length $L = 0.1\,\mu$m (and $L_y = 0.1\,\mu$m, $L_z = 2\,\mu$m) or $L = 1\,\mu$m (and $L_y = 1\,\mu$m, $L_z = 20\,\mu$m) and a maximal doping of $10^{22}\,\mathrm{m}^{-3}$. The remaining physical parameters are listed in Table 4.1. The resistance in the circuit equals $R = 100\,\Omega$ and the voltage source is given by $v(t) = U_0 \sin(2\pi\omega t)$ with $U_0 = 5\,\mathrm{V}$ and $\omega = 1\,\mathrm{GHz}$ or $\omega = 10\,\mathrm{GHz}$.

h/L	$RE(n)$	$RE(w)$	$RE(p)$	$RE(V)$	$RE(T)$	$RE(j_S)$	$RE(circuit)$
0.04	$8.7 \cdot 10^{-2}$	$1.3 \cdot 10^{-1}$	$6.8 \cdot 10^{-2}$	$2.3 \cdot 10^{-2}$	$1.0 \cdot 10^{-1}$	$1.1 \cdot 10^{-1}$	$1.5 \cdot 10^{-2}$
0.02	$3.5 \cdot 10^{-2}$	$5.3 \cdot 10^{-2}$	$2.7 \cdot 10^{-2}$	$1.2 \cdot 10^{-2}$	$7.3 \cdot 10^{-2}$	$5.0 \cdot 10^{-2}$	$6.9 \cdot 10^{-3}$
0.01	$1.1 \cdot 10^{-2}$	$1.7 \cdot 10^{-2}$	$8.0 \cdot 10^{-3}$	$4.1 \cdot 10^{-3}$	$4.7 \cdot 10^{-2}$	$1.7 \cdot 10^{-2}$	$2.3 \cdot 10^{-3}$
0.005	$2.4 \cdot 10^{-3}$	$3.9 \cdot 10^{-3}$	$1.8 \cdot 10^{-3}$	$1.1 \cdot 10^{-3}$	$2.3 \cdot 10^{-2}$	$4.1 \cdot 10^{-3}$	$5.7 \cdot 10^{-4}$
rate	1.73	1.67	1.75	1.47	0.72	1.60	1.59

TABLE 4.2

Relative error (RE) for different space step sizes. The time step size is $\triangle t = 10^{-12} s$.

$\triangle t$	$RE(n)$	$RE(\epsilon)$	$RE(p)$	$RE(V)$	$RE(T)$	$RE(j_S)$	$RE(circuit)$
10	$2.0 \cdot 10^{-3}$	$1.6 \cdot 10^{-3}$	$1.9 \cdot 10^{-3}$	$6.0 \cdot 10^{-4}$	$5.6 \cdot 10^{-3}$	$2.1 \cdot 10^{-3}$	$3.6 \cdot 10^{-4}$
8	$1.5 \cdot 10^{-3}$	$1.1 \cdot 10^{-3}$	$1.4 \cdot 10^{-3}$	$5.2 \cdot 10^{-4}$	$4.5 \cdot 10^{-3}$	$1.6 \cdot 10^{-3}$	$3.0 \cdot 10^{-4}$
5	$7.3 \cdot 10^{-4}$	$5.7 \cdot 10^{-4}$	$6.8 \cdot 10^{-4}$	$3.5 \cdot 10^{-4}$	$2.8 \cdot 10^{-3}$	$1.5 \cdot 10^{-3}$	$2.2 \cdot 10^{-4}$
4	$5.5 \cdot 10^{-4}$	$4.1 \cdot 10^{-4}$	$5.1 \cdot 10^{-4}$	$3.1 \cdot 10^{-4}$	$2.7 \cdot 10^{-3}$	$1.4 \cdot 10^{-3}$	$1.8 \cdot 10^{-4}$
rate	1.38	1.51	1.41	0.66	0.76	0.56	0.74

TABLE 4.3

Relative error (RE) for different time step sizes. The space step size is $h = 0.0025L$*;* $\triangle t$ *is measured in units of* 10^{-13} *s.*

We use the same initial conditions as in the previous subsection. For the Graetz bridge, we may employ Dirichlet or Robin boundary conditions as these conditions effect the behavior of the temperature on the boundary but less the current values. Only the profile of the electron density changes slightly. Here, for simplicity, we have employed Robin conditions with large values for α and β, which almost gives Dirichlet conditions.

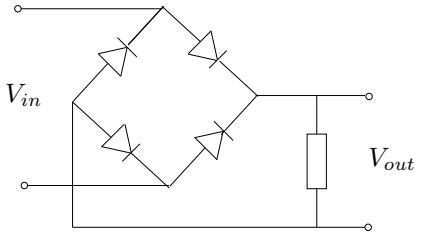

FIG. 4.6. *Rectifier circuit.*

The numerical simulations are performed on a uniform grid with 51 nodes for each diode. For simplification, we employed the constant time step 0.5 ps. This time step is needed for accurate computations for the diodes at reverse bias and at the switching point. The implementation of an time-adaptive grid would generally allow to choose much larger time steps.

The numerical convergence is tested on a numerical solution on a fine grid with 401 nodes and time step $\triangle t = 5 \cdot 10^{-14}$ s. The reference solution simulates the circuit during one oscillation in the time interval $[0, 10^{-10}\,\mathrm{s}]$. In Tables 4.2 and 4.3 the relative errors with respect to the L^2 norm and the numerical convergence orders are depicted. Recall that $w = \frac{3}{2}nT$ denotes the thermal energy. The relative error *RE(circuit)* of the circuit is the L^2-error of the node potentials and the branch current.

The spatial convergence orders for the densities and the temperature are slightly smaller than those obtained for the uncoupled energy-transport equations [23] which shows that the coupling plays an important role. The temperature T is obtained from

the electron density n and the energy density w by averaging the quantity $T = 2w/3n$, which may explain the rather low convergence order of T. The temporal convergence orders are smaller than those with respect to space discretization, probably due to the coupling.

In Figure 4.7 the energy density in one of the diodes during one oscillation of the circuit for two different device sizes and frequencies is presented. Here, we observe that the energy density is higher for the larger device.

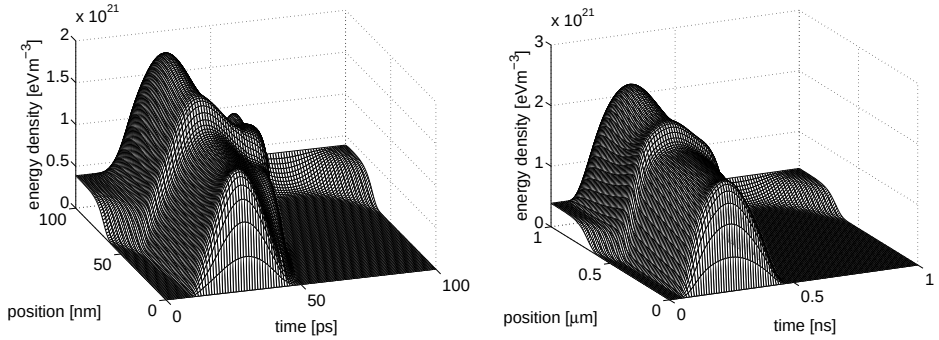

FIG. 4.7. *Energy density in a pn diode with size $L = 0.1\,\mu m$ and frequency $10\,GHz$ (left); $L = 1\,\mu m$ and frequency $1\,GHz$ (right). The maximal doping is $10^{22}\,m^{-3}$.*

Next, we investigate the behavior of the current through one diode and through the circuit using the transient or stationary energy-transport equations (ET) and the transient drift-diffusion model (DD). Figure 4.8 shows the current from simulations of a $1\,\mu$m diode in a 1 GHz circuit. The figure clearly shows the rectifying behavior of the circuit. The largest current is obtained from the drift-diffusion model since we have assumed a constant electron mobility such that the drift is unbounded with respect to the modulus of the electric field. The stationary energy-transport model is not able to catch the capacitive effect at the junction. Similar statements hold for the output signal of the circuit.

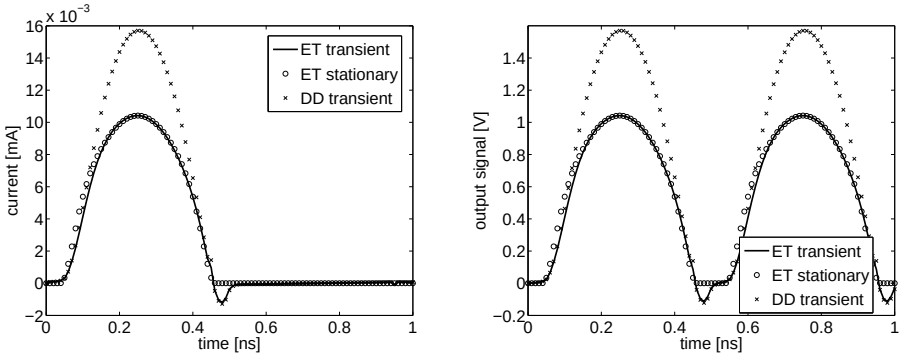

FIG. 4.8. *Left: Current through a $1\,\mu m$ diode in a $1\,GHz$ circuit. Right: Output signal of the circuit.*

Finally, we consider a Graetz bridge with a larger frequency of 10 GHz and smaller device size of $0.1\,\mu$m. The current through one of the diodes of the circuit and the output signal of the circuit is presented in Figure 4.9. Here, the differences between

the three models are more pronounced. Clearly, the capacitive effect is larger for this rather high frequency. As in the previous example, the stationary model cannot capture this effect. Moreover, we observe a slight time shift between the stationary and the transient energy-transport equations.

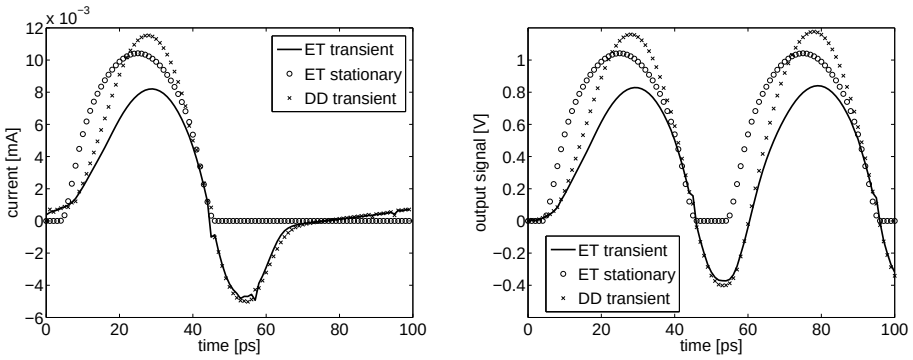

FIG. 4.9. *Left: Current through a* $0.1\,\mu m$ *diode in a 10 GHz circuit. Right: Output signal of the circuit.*

5. Conclusion. In this paper we have presented for the first time the numerical coupling of the transient energy-transport model for semiconductor devices with circuit equations from modified nodal analysis, leading to a system of partial differential-algebraic equations. The numerical comparison with the drift-diffusion model shows the strong influence of the carrier heating on the current density. In some physical situations, the stationary energy-transport model seems to provide reasonable results, compared to the other two models. However, in high-frequency circuits, the use of the transient model seems to be necessary.

We have also compared the effect of the boundary conditions for the device. Boundary layers which appear when standard Dirichlet conditions for the particle density and energy density are employed disappear if appropriate Robin boundary conditions for these variables are used.

Notice that we have only considered the heating of the electrons, and the lattice temperature is assumed to be constant. Clearly, the hot-electron flow will influence the lattice temperature and heat up the semiconductor device. This modeling is important to identify hot spots in VLSI design. The transfer of thermal energy can be modeled, for instance, by a heat equation for the lattice temperature which couples through a relaxation-time term to the electron temperature (see, e.g. [49] or chapter 3.1.4. in [19]). The numerical solution of the corresponding coupled model will be performed in a future work.

REFERENCES

[1] G. Alì, A. Bartel, and M. Günther. Parabolic differential-algebraic models in electrical network design. *Multiscale Model. Simul.* 4 (2005), 813-838.

[2] G. Alì, A. Bartel, M. Günther, and C. Tischendorf. Elliptic partial differential-algebraic multiphysics models in electrical network design. *Math. Models Meth. Appl. Sci.* 13 (2003), 1261-1278.

[3] D. Arnold. MIxed finite element methods for elliptic problems. *Comput. Meth. Appl. Mech. Engin.* 82 (1990=, 281-300.

[4] A. Bartel and M. Günther. Multirate co-simulation of first order thermal models in electric

circuit design. In: W. Schilders et al. (eds.), *Scientific Computing in Electrical Engineering*. Proceedings SCEE 2002, Eindhoven, Netherlands. Springer, Berlin (2002),23-28.
[5] N. Ben Abdallah and P. Degond. On a hierarchy of macroscopic models for semiconductors. *J. Math. Phys.* 37 (1996), 3308-3333.
[6] M. Bodestedt. *Index Analysis of Coupled Systems in Circuit Simulatiom*. Licentiate Thesis, Lund University, Sweden, 2004.
[7] M. Bodestedt and C. Tischendorf. PDAE models for integrated circuits and perurbation analysis. To appear in *Math. Comput. Model. Dynam. Sys.*, 2007.
[8] F. Bosisio, R. Sacco, F. Saleri, and E. Gatti. Exponentially fitted mixed finite volumes for energy balance models in semiconductor device simulation. In: H. Bock et al. (eds.), *Proceedings of ENUMATH 97*, World Scientific, Singapure (1998), 188-197.
[9] K. Brennan, S. Campell, and L. Petzold. *Numerical Solution of Initial-Value Problems in Differential-Algebraic Equations*. North-Holland, New York, 1989.
[10] F. Brezzi, L. Marini, S. Micheletti, P. Pietra, R. Sacco, and S. Wang. Discretization of semiconductor device problems. In: W. Schilders and E. ter Maten (eds.), *Handbook of Numerical Analysis. Numerical Methods in Electromagnetics*. Elsevier, Amsterdam, Vol. 13 (2005), 317-441.
[11] D. Chen, E. Kan, U. Ravaioli, C. Shu, and R. Dutton. An improved energy transport model including nonparabolicity and non-Maxwellian distribution effects. *IEEE Electr. Dev. Letters* 13 (1992), 26-28.
[12] P. Degond. Mathematical modelling of microelectronics semiconductor devices. In: L. Hsiao (ed.), *Some Current Topics on Nonlinear Conservation Laws*. Amer. Math. Soc., Providence, USA (2000), 77-100.
[13] P. Degond, A. Jüngel, and P. Pietra. Numerical discretization of energy-transport models for semiconductors with non-parabolic band structure. *SIAM J. Sci. Comp.* 22 (2000), 986-1007.
[14] P. Degond, S. Génieys, and A. Jüngel. A system of parabolic equations in nonequilibrium thermodynamics including thermal and electrical effects. *J. Math. Pures Appl.* 76 (1997), 991-1015.
[15] K. Einwich, P. Schwarz, P. Trappe, and H. Zojer. Simulatorkopplung für den Entwurf komplexer Schaltkreise der Nachrichtentechnik. In: 7. ITG-Fachtagung "Mikroelektronik für die Informationstechnik", Chemnitz (1996), 139-144.
[16] A. Forghieri, R. Guerrieri, P. Ciampolini, A. Gnudi, M. Rudan, and G. Baccarani. A new discretization strategy of the semiconductor equations comprising momentum and energy balance. *IEEE Trans. Computer-Aided Design Integr. Circuits Sys.* 7 (1988), 231-242.
[17] M. Fournié. Numerical discretization of energy-transport model for semiconductors using high-order compact schemes. *Appl. Math. Lett.* 15 (2002), 727-734.
[18] H. Gajewski and K. Gröger. Semiconductor equations for variable mobilities based on Boltzmann statistics or Fermi-Dirac statistics. *Math. Nachr.* 140 (1989), 7-36.
[19] T. Grasser. *Mixed-Mode Device Simulation*. PhD thesis, Vienna University of Technology, Austria, 1999.
[20] K. Gröger. Initial boundary value problems from semiconductor device theory. *Z. Angew. Math. Mech.* 67 (1987), 345-355.
[21] M. Günther. A PDAE model for interconnected linear RLC networks. *Math. Computer Modeling Dynam. Sys.* 7 (2001), 189-203.
[22] E. Hairer and G. Wanner. *Solving Ordinary Differential Equations II*. Springer, Berlin, 1991.
[23] S. Holst, A. Jüngel, and P. Pietra. A mixed finite-element discretization of the energy-transport equations for semiconductors. *SIAM J. Sci. Comp.* 24 (2003), 2058-2075.
[24] S. Holst, A. Jüngel, and P. Pietra. An adaptive mixed scheme for energy-transport simulations of field-effect transistors. *SIAM J. Sci. Comp.* 25 (2004), 1698-1716.
[25] J. Jerome and C.-W. Shu. Energy models for one-carrier transport in semiconductor devices. In: W. Coughran et al. (eds.), *Semiconductors, Part II*, Springer, New York (1994), 185-207.
[26] A. Jüngel and S. Tang. Numerical approximation of the viscous quantum hydrodynamic model for semiconductors. *Appl. Numer. Math.* 56 (2006), 899-915.
[27] C. Lab and P. Caussignac. An energy-transport model for semiconductor heterostructure devices: application to AlGaAs/GaAs MODFETs. *COMPEL* 18 (1999), 61-76.
[28] R. Lamour. Index determination and calculation of consistent initial values for DAEs. *Computers Math. Appl.* 50 (2005), 1125-1140.
[29] R. März. Numerical methods for differential-algebraic equations. *Acta Numerica* (1992), 141-198.
[30] R. März. Differential algebraic systems anew. *Appl. Numer. Math.* 42 (2002), 315-335.
[31] I. Hiqueras and R. März. Differential algebraic systems with properly stated leading terms.

Comput. Math. Appl. 48 (2004), 215-235.
[32] L. D. Marini and P. Pietra. An abstract theory for mixed approximations of second order elliptic equations. *Mat. Aplic. Comp.* 8 (1989), 219-239.
[33] L. D. Marini and P. Pietra. New mixed finite element schemes for current continuity equations. *COMPEL* 9 (1990), 257-268.
[34] A. Marrocco and P. Montarnal. Simulation of energy-transport models via mixed finite elements. *C. R. Acad. Sci., Paris, Sér. I* 323 (1996), 535-541.
[35] J. Litsios, B. Schmithüsen, U. Krumbein, A. Schenk, E. Lyumkis, B. Polsky, and W. Fichtner. *DESSIS 3.0 Manual*. ISE Integrated Systems Engineering, Zürich, 1996.
[36] K. Pipe, R. Ram, and A. Shakouri. Bias-dependent Peltier coefficient and internal heating in bipolar devices. *Phys. Rev. B* 66 (2002), 125316.
[37] P. Raviart and J. Thomas. A mixed finite element method for second order elliptic equations. In: *Mathematical Aspects of the Finite Element Method*, Proc. Conf. Rome 1975. Lecture Notes in Mathematics 606 (1977), 292-315.
[38] C. Ringhofer. An entropy-based finite difference method for the energy transport system. *Math. Models Meth. Appl. Sci.* 11 (2001), 769-796.
[39] F. Rotella. *Mixed circuit and device simulation for analysis, design, and optimization of optoelectronic, radio frequency, and high speed semiconductor devices.* PhD thesis, Stanford University, 2000.
[40] M. Rudan, A. Gnudi, and W. Quade. A generalized approach to the hydrodynamic model of semiconductor equations. In: G. Baccarani (ed.), *Process and Device Modeling for Microelectronics*, Elsevier, Amsterdam (1993), 109-154.
[41] D. Schroder. Carrier lifetimes in silicon. *IEEE Trans. Electron Dev.* 44 (1997), 160-170.
[42] M. Selva Soto and C. Tischendorf. Numerical analysis of DAEs from coupled circuit and semiconductor simulation. *Appl. Numer. Math.* 53 (2005), 471-488.
[43] K. Souissi, F. Odeh, H. Tang, and A. Gnudi. Comparative studies of hydrodynamic and energy transport models. *COMPEL* 13 (1994), 439-453.
[44] R. Stratton. Diffusion of hot and cold electrons in semiconductor barriers. *Phys. Rev.* 126 (1962), 2002-2014.
[45] C. Tischendorf. *Solution of Index-2 Differential-Algebraic Equations and Its Application to Circuit Simulation.* PhD thesis, Humboldt-Universität zu Berlin, 1996.
[46] C. Tischendorf. Topological index calculation of differential-algebraic equations in circuit simulation. *Surveys Math. Industr.* 8 (1999), 187-199.
[47] C. Tischendorf. Modeling circuit systems coupled with distributed semiconductor equations. In: K. Antreich, R. Bulirsch, A. Gilg, and P. Rentrop (eds.), *Modeling, Simulation, and Optimization of Integrated Circuits*, Internat. Series Numer. Math. 146 (2003), 229-247.
[48] C. Tischendorf. Coupled systems of differential algebraic and partial differential equations in circuit and device simulations. Habilitation thesis, Humboldt Universität zu Berlin, 2003.
[49] G. Wachutka. Rigorous thermodynamic treatment of heat generation and conduction in semiconductor device modeling. *IEEE Trans. Computer-Aided Design* 9 (1990), 1141-1149.
[50] A. Yamnahakki. Second-order boundary conditions for the drift-diffusion equations for semiconductors. *Math. Models Meth. Appl. Sci.* 5 (1995), 429-455.